Pattern Detection for Toolpath Generation on Triangular Meshes for 5-Axis CNC machining

Le V. Dang[1] 🆔, Samart Moodleah[2] 🆔 and Stanislav S. Makhanov[1] 🆔

[1]SIIT, Thammasat University, Rangsit, Pathum Thani, 12000, Thailand

[2]King Mongkut's Institute of Technology Ladkrabang, Bangkok, 10520, Thailand

Corresponding author: Stanislav S. Makhanov, makhanov@siit.tu.ac.th

Abstract. Toolpath generation for freeform triangular meshes for 5-axis milling machines using an optimal feeding direction (OFD) field is an important topic in subtractive manufacturing technology. By considering parameters in both the CAD and the CAM stages, there exists a direction(s) at every cutter contact (CC) point, such that the machining efficiency is maximal. The directions could form a special structure which can be detected for toolpath generation on the CAD stage. In this paper, a novel toolpath generation method is proposed to create a toolpath for freeform triangular meshes by detecting regular structures of the OFD in the parametric domain using moment invariants. Three common templates, corresponding to standard toolpath structures, are considered: (1) curl (contour/spiral contour path), (2) star/spiral (radial path), and (3) shear (zigzag path). Mesh parameterization is used to flatten the 3D triangulated surface. A transfinite interpolation (TFI) is utilized to construct the toolpath on the flattened surface. The final toolpath is then obtained by the inverse map. The proposed method has been compared with conventional and standard commercial toolpaths. Numerical results show that the pattern detection algorithm helps to find an appropriate toolpath strategy. The generated toolpaths follow the OFDs closer than the competing methods, and therefore, require shorter machining time.

1   INTRODUCTION

Five-axis machining technology is an important area of the precision automotive industry since it is able to produce complex and smooth surfaces with high accuracy. The toolpath is often required for surfaces presented in specific industrial formats such as NURBS, B-Splines, STL, STEP, etc. Toolpath generation of freeform triangulated surfaces given in the STL format is important in 5-axis machining research due to the availability of 3D scanning and finite element analysis.

A common approach, to generate a toolpath for an STL surface, is curve offsetting. An initial curve (a boundary or some other particular curve on the surface) is generated. The adjacent path is generated by offsetting the previous path using the scallop height constraint. The popular offset approaches are the iso-planar, iso-scallop, iso-phote, and iso-parametric path methods [10]. The first three methods often generate sharp turns, self-intersections, and high redundancy [24]. The iso-parametric method requires parameterization (flattening). Although a distortion-free mesh flattening method does not exist [20], there are many popular types of parameterizations. The harmonic map [20] is considered a good choice since it minimizes the angular distortions.

The toolpath generation strategy is often selected based on the features of the part surface, machine configuration, and experience of the CNC programmer. The idea of the toolpath following a certain optimal vector field has been discussed for decades [3]. The OFD at each cutter contact (CC) point is generated by a set of utility (cost) functions. These cost functions may include machining strip, kinematic error, scallop height, avoidance of the local and global collisions, maximum feed rates for each axis, and other machining conditions [7]. In other words, if the tool follows the OFD at each CC point and the redundancy is low, the required machining efficiency can be achieved. However, it is usually not possible to connect the CC points following the OFD field, given that the toolpath should be continuous, not redundant, and self-intersection free [22]. Therefore, the problem can be formulated as to align the toolpath with the OFDs at as many CC points as possible [8].

In general, the most popular toolpath topologies are the zigzag, contour, and spiral [10], possibly combined with a decomposition of the surface. The practical implementation is not a simple task. Inappropriate toolpaths create a large number of turning points, large kinematic errors, high redundancy, undesirable high angular variations, etc.

The proposed strategy is based on the complex moment invariants and template patterns. These are used as a library to help in detecting suitable structures for the toolpath generation. The proposed moments are scale and rotation invariant [4], which makes it possible to generate an efficient decomposition of the surface into subsurfaces. An appropriate toolpath from the library is then applied to each subsurface. Our tests against the conventional methods show some advantages of the proposed methodology. This paper is organized as follows. Section 2 introduces the proposed model. Section 3 presents the numerical experiments and discussion. The conclusions are given in Section 4.

2   TOOLPATH GENERATION

2.1   Vector Field Generation

The OFD field can be defined in terms of the maximal cutting strip width [9,12,13], maximal material removal rate (MRR) [7], [26], [17], minimal cutting force [14], etc. Our model is applied to the MRR OFD field. The OFD fields (based on other utility functions) can be constructed similarly. The MRR OFD field for the STL surface is constructed as follows.

First, all vertices of the triangular mesh are considered as CC points. From each vertex v_i, a geodesic disk with a small radius is selected. A set of sample points on the disk is generated. The sample feed directions are a set of vectors from the center of the disk to the sample points (Figure 1(a)). The corresponding machining strip width for a ball-end mill with radius r is given by [15]:

$$w_i = \sqrt{\frac{8hrR}{R-r}} \, , \qquad (2.1)$$

where h is the maximum allowable scallop height, and R is the normal curvature of the surface at v_i ($R > 0$ for a concave surface and $R < 0$ for a convex surface). Several techniques can be applied to calculate the curvature on a triangular mesh [22], [26]. In this work, the averaging tensor technique proposed in [18] is used.

Let F_0 be the programmed feed rate. The MRR in the feed direction f_i is determined by:

$$MRR(f_i) = F_0 w_i. \tag{2.2}$$

During the machine operation process, the programmed feed rate may exceed the maximum feed rate of a certain axis. In this case, it is automatically reassigned by the machine controller [26]. Let W^* be a sample point on the corresponding geodesic disk such that $MRR(\overrightarrow{v_i W^*})$ is maximal. The vector $f_i^* = \overrightarrow{v_i W^*}$ is then the desired optimal MRR direction (Figure 1(a)). The MRR vectors are transferred into the parametric domain using the harmonic map [25]. Examples of an OFD field on a 3D triangular mesh and the parametric domain are given in Figure 1(b) and Figure 1(c). Note that the OFD is a bidirectional vector field since forward and backward cutting does not affect the machine efficiency [13]. By applying barycentric interpolation [2], a piecewise discrete orientation field (OF) is obtained (see Figure 1(d)). Our next task is to classify the OF so that an appropriate toolpath can be generated.
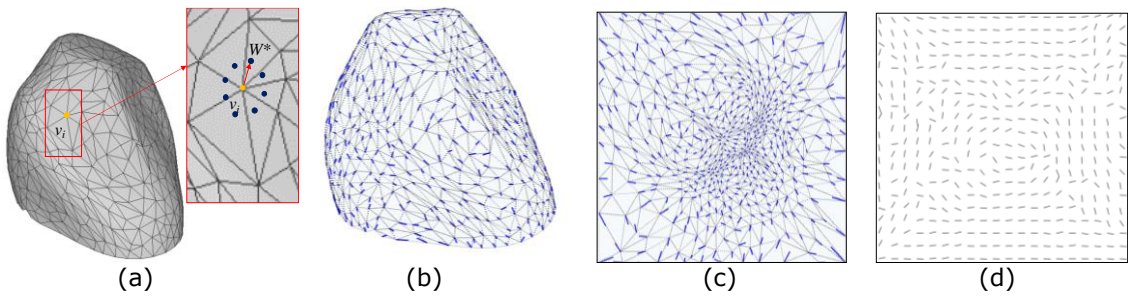

Figure 1: OF generation process.

2.2   Pattern Detection Using the Moment Invariants

Let us represent the OF as a set of complex numbers $V = v_x + iv_y$. Define

$$\theta(x,y) = \begin{cases} \arctan\left(\dfrac{v_y}{v_x}\right), \text{if } v_x \neq 0, \\ -\dfrac{\pi}{2}, \text{otherwise.} \end{cases} \tag{2.3}$$

Clearly, $\theta(x,y) = \theta(-x,-y)$ and $\theta(-x,y) = \theta(x,-y)$. Therefore, $f(x,y) = e^{i\theta(x,y)}$ is "flip invariant" and can represent the OF. In practice, the argument $\theta(x,y)$ is doubled ($\hat{f}(x,y) = e^{i2\theta(x,y)}$) to exclude the cancellation of opposite vectors during the integration [11].

A moment c_{pq} of an integrable complex function $\hat{f}(x,y)$ is given by [4]:

$$c_{pq} = \int_{-\infty}^{\infty}\int_{-\infty}^{\infty} (x+iy)^p (x-iy)^q \hat{f}(x,y) dx dy. \tag{2.4}$$

The integral $\int_{-\infty}^{\infty}\int_{-\infty}^{\infty}$ is replaced by a summation over a sampling square window with side R_s. Fortunately, the most important information about the OF is represented by the low order moments. Following [19], we use a set of independent moments of the order $p+q \leq 2$:

$$M = \{c_{01}, c_{00}c_{02}, c_{11}c_{02}, c_{10}c_{02}^2, c_{20}c_{02}^3\}. \tag{2.5}$$

To classify the patterns, we compare the moment vector M with the moment M_0 of a template, using the classification threshold ζ [6]. Table 1 shows the test results of the classifying synthetic patterns, e.g., star, curl, spiral, and shear, shown in Figure 2(a)-Figure 2(d). The synthetic patterns have been degraded by Gaussian noise with a zero mean and standard deviation $\sigma = 0.2, 0.3,$ and 0.4 [21]. The classification has been verified using 50 random samples for each configuration.
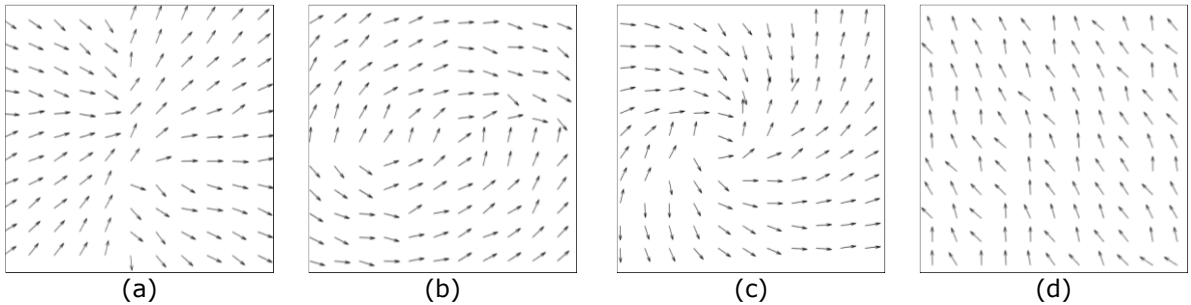

| (a) | (b) | (c) | (d) |

Figure 2: Template pattern library.

A moving square window centered at a cell (i, j) of the parametric domain is defined. For each position (i, j) a vector of invariant moments $M_{i,j}$ is evaluated. The window size is a fraction of the size of the OF. In practice, we apply a window with size equal to $\frac{2}{3}$ of the OF. The template which satisfies $\| M_{i,j} - M_0 \| \leq \zeta$ is selected. For practical calculations, we consider $\zeta = 0.15$.

Pattern	*Standard deviation* σ		
	$\sigma = 0.2$	$\sigma = 0.3$	$\sigma = 0.4$
Star	100	98	86
Curl	100	94	88
Spiral	98	96	84
Shear	98	92	90
Average rate	99	95	87

Table 1: Detection rate of template patterns using moment invariants.

2.3   Grid Generation

The TFI grid is characterized by fast execution, minimal input effort, automatic node connectivity, and good correlation between the boundary nodes and the interior mesh [5]. By means of selecting the boundaries, different grid structures can be obtained. We consider three basic structures, i.e., the O-gird, C-grid, and H-grid. The corresponding toolpaths are the contour or radial path, C-type zigzag path, and H-type zigzag path [16].

Let $\Delta = \{0 \leq \xi \leq 1, \, 0 \leq \eta \leq 1\}$ be a computational region. The grid is a mapping from Δ onto a region D in the parametric coordinates (u, v). Let $R_k(\xi)$, $k = \overline{0, N_\eta}$, $T_p(\eta)$, $p = \overline{0, N_\xi}$ be the boundary and the inner coordinate curves in parametric space (u, v) to be transformed into computational space (ξ, η) (Figure 3).

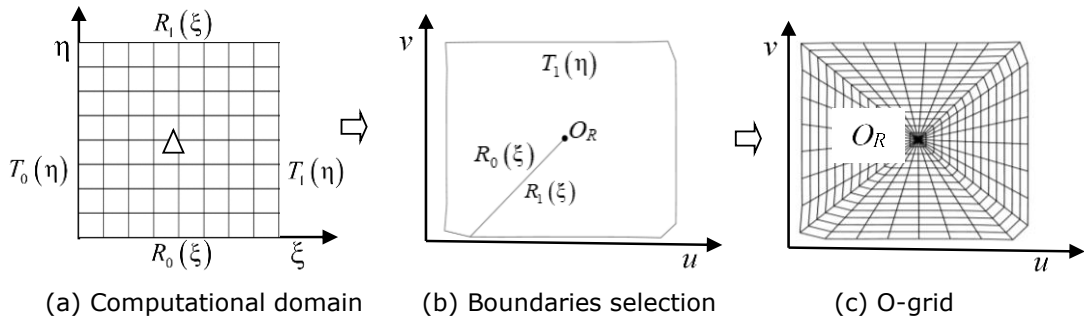(a) Computational domain   (b) Boundaries selection   (c) O-grid

Figure 3: Grid generation.

Define the coordinate transformation by

$$F(\xi,\eta) \equiv (u(\xi,\eta),v(\xi,\eta)) = \sum_p T_p(\eta)\psi_p(\xi) + \sum_k R_k(\xi)\varphi_k(\eta) - \sum_k \sum_p T_p(\eta_k)\psi_p(\xi)\varphi_k(\eta),$$ (2.6)

where $\psi_p(\xi)$, $\varphi_k(\eta)$ are blending functions such that

$$\psi_p(\xi_i) = \begin{cases} 1, & p = i, \\ 0, & \text{otherwise,} \end{cases}, \varphi_k(\eta_j) = \begin{cases} 1, & k = j, \\ 0, & \text{otherwise.} \end{cases} \quad i = \overline{0,N_\xi}, \ j = \overline{0,N_\eta}.$$

Clearly,

$$F(\xi,\eta_k) = R_k(\xi), \ k = \overline{0,N_\eta},$$
$$F(\xi_p,\eta) = T_p(\eta), \ p = \overline{0,N_\xi}.$$ (2.7)

Let us illustrate the selection of the boundaries for the curl pattern. Denote the center of the OF by O_R (Figure 3). Consider the simplest case $N_\xi = N_\eta = 1$. The boundaries and the blending functions are then given by $\xi_0 = \eta_0 = 0, \xi_1 = \eta_1 = 1$, $\psi_0(\xi) = 1-\xi$, $\psi_1(\xi) = \xi$, $\varphi_0(\eta) = 1-\eta$, and $\varphi_1(\eta) = \eta$. The TFI generates the O-grid defined by $T_0(\eta), T_1(\eta)$, $R_0(\xi) = R_1(\xi)$. Note that $O_R = T_0(\eta)$ is a curve degenerated to a single point, while $R_0(\xi) = R_1(\xi)$ is a linear cut connecting O_R and the boundary $T_1(\eta)$. The O-grid makes it possible to generate the radial zigzag, contour, and spiral toolpaths.

To construct the H-grid, the OF is rotated by an angle α around the centroid (i,j), as shown in Figure 4. The rectangular bounding box of the rotated OF is evaluated. The H-grid is generated using the resulting boundaries. Figure 4 shows an example of the O-grid and H-grid aligned with the OF radial toolpath, and the shear patterns and the corresponding toolpaths.

The interval between the tracks is adapted by bisection. The Hausdorff distance between the neighboring tracks, $P_i(\xi) = S(F(\xi,\eta_i))$ and $P_{i+1}(\xi) = S(F(\xi,\eta_{i+1}))$, is evaluated. If $\text{dist}_H\ P_i,P_{i+1} \geq w_i$, where w_i is the maximum possible machining strip width (path interval which is calculated using Equation (2.1)), a new grid line is inserted. The corresponding path structure is extracted from the 2D grid and mapped back onto the 3D mesh to receive the CC path. The tool orientations are modified to avoid gouging and to obtain smooth rotary transitions. The corresponding cutter locations are now determined and converted to G-code using the kinematics transformation of the machine [15].
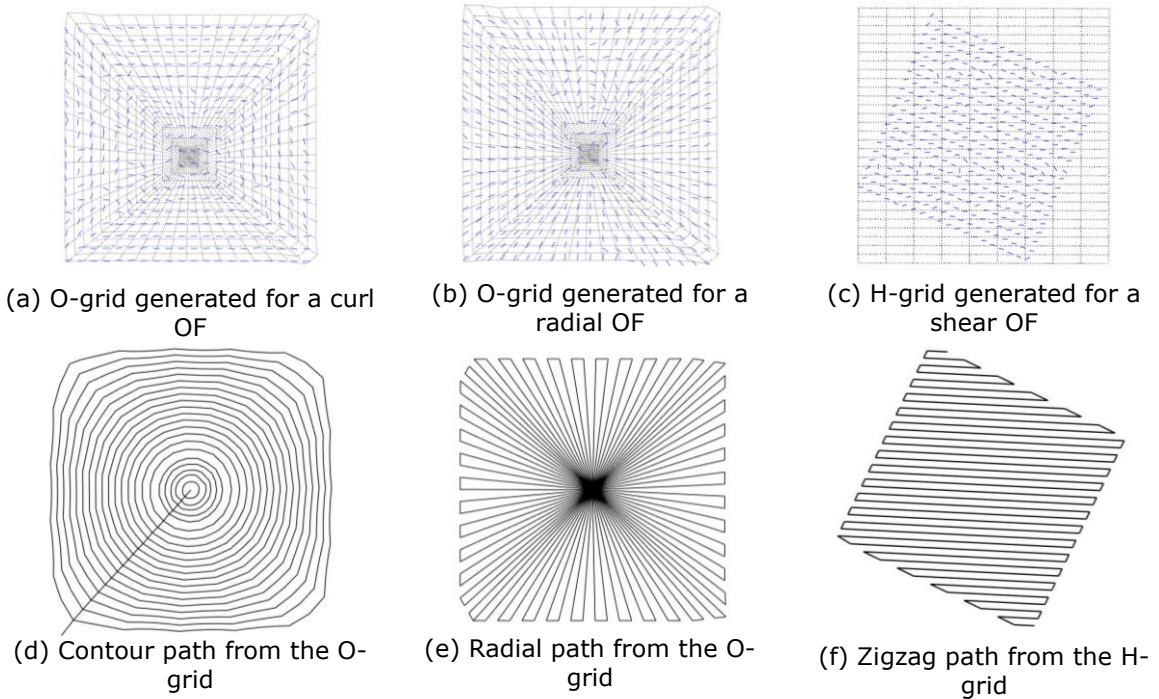
(a) O-grid generated for a curl OF

(b) O-grid generated for a radial OF

(c) H-grid generated for a shear OF

(d) Contour path from the O-grid

(e) Radial path from the O-grid

(f) Zigzag path from the H-grid

Figure 4: O-grid and H-grid generation aligned OFs.

Let $P = CC_k, k = 1, 2, ..., N_{CC}$ be the generated toolpath. Recall that when the programmed feed rate F_0 exceeds the machining capacity of the axis, the maximal feed rate of the machine is automatically used instead. Thus, the actual feed rate is evaluated by [7]

$$F_k = \min\left(F_0, \min_a\left(\frac{v_a^* l_{CC_k}}{d_{a,k}}\right)\right), \tag{2.8}$$

in which l_{CC_k} is the length of the machining curve between CC_k and CC_{k+1}. $d_{a,k}$ and v_a^* are the travelling distance and maximum velocity of axis *a* (linear or angular). The total machining time is then

$$T = \sum_{k=1}^{N_{CC}-1} t_k, \tag{2.9}$$

where $t_k = \dfrac{l_{CC_k}}{F_k}$ and N_{CC} is the number of CC points.

3   NUMERICAL EXPERIMENTS

In this section, the proposed method is applied to generate toolpaths for two STL surfaces. The synthetic STL surfaces have been generated using parametric equations and a MATLAB library [23]. To compare with commercial software, the surface has been converted into a solid model for 5-axis toolpath generation in NX11.0 [28]. Note that NX11.0 and other commercial software still do not

support toolpath generation for multi-axis machining of the STL format. The second example is an STL model of a crown for a molar tooth.

The toolpaths have been designed for the table/titling 5-axis milling machine, HAAS VF 2TR. The kinematics transformation [15] is used for this type of machine. The tool is aligned with the normal vector. The feed rates, $F_0 = 35\,\mathrm{mm/s}$ and $F_0 = 10\,\mathrm{mm/s}$, are used for surface 1 and 2, respectively. The ball-end mill radius is $2\,\mathrm{mm}$, and the maximum allowable scallop height $h = 0.1\,\mathrm{mm}$. The improvement of machining time (%) between the proposed method and competitive methods are calculated for each test.

3.1 Example 1: Synthetic STL surface

The synthetic STL surface and its OF are given in Figure 5(a) and Figure 5(b). The pattern detection algorithm classifies the OF as the shear pattern with the orientation $\alpha = 30^0$, relative to the reference horizontal axis. Table 2 shows the OF detection results.

Similarity at sample points	Template			
	Curl	Star	Spiral	Shear
$\|\| M_{i,j} - M_0 \|\|$	0.0969	0.0994	0.1110	**0.0026**
	0.1006	0.1044	0.1120	0.0104
	0.1038	0.1069	0.1159	0.0123
	0.1038	0.1090	0.1488	0.0674

Table 2: Pattern detection for the synthetic surface.

The proposed method is compared with the iso-parametric paths (Figure 5(c), Figure 5(d)), and a toolpath generated in NX11 (following periphery (FP) option, Figure 5(e)). The proposed toolpath is shown in Figure 5(f). The proposed toolpath closely follows the OF even though it is not well aligned for a few points at the peaks (see Figure 5(b) and Figure 5(f)). Table 3 compares the methods, numerically.

Method	Scallop height, h=0.1(mm)			
	# of CC points	Length (mm)	Time (s)	Time improvement (%)
Iso-parametric u	4210	$2.55\ 10^4$	467.6	78.31
Iso-parametric v	4811	$0.87\ 10^3$	561.9	81.95
NX11.0 (FP)	5547	$0.10\ 10^3$	658.9	**84.61**
Proposed method	**1963**	**$0.53\ 10^3$**	**101.4**	-

Table 3: Machining time of the synthetic STL surface.

The results indicate that the proposed method outperforms the reference methods, in particular compared with the toolpath created by NX11.0 (using FP option). In multi-axis machining, the fastest feed rate is usually along the lowest curvature. Therefore, the majority of optimal vectors are along this direction. When the curvature is low, the tool moves almost linearly. Since the proposed toolpath automatically follows this algorithm, the number of required CC points is the smallest compared to the other methods (Table 3).
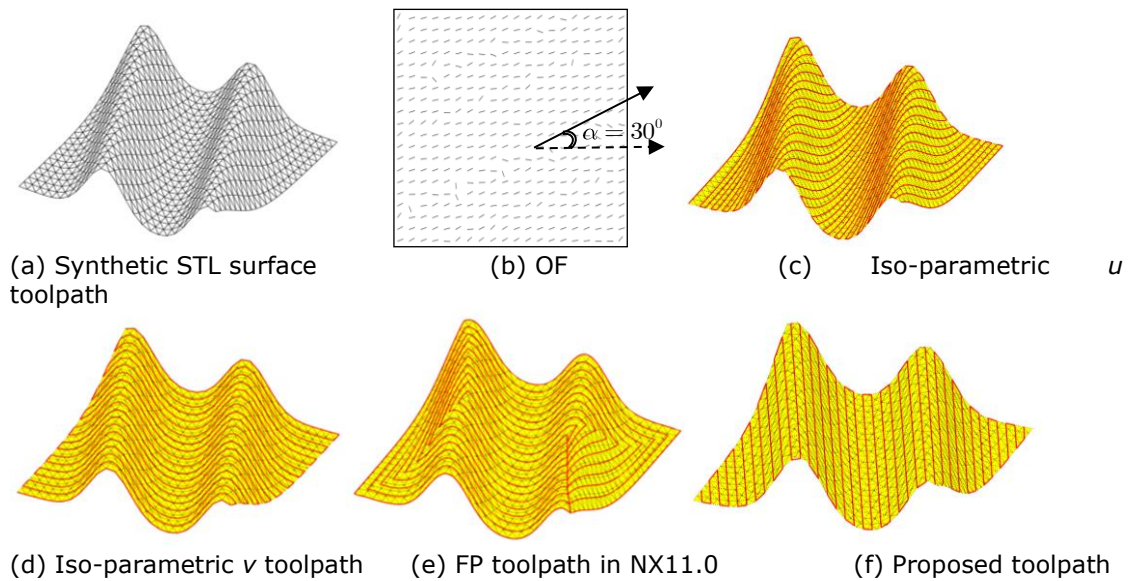
(a) Synthetic STL surface toolpath

(b) OF

(c) Iso-parametric *u*

(d) Iso-parametric *v* toolpath

(e) FP toolpath in NX11.0

(f) Proposed toolpath

Figure 5: Toolpath generation for the synthetic triangular mesh.

3.2 Example 2: Crown for a Molar Tooth

Figure 6(a) and Figure 6(b) show the STL model of a crown tooth and its MRR-OF, respectively. Visually, the OF is closely aligned with the curl pattern although the MRR directions in the central area are chaotic. Table 4 shows the detection results. It indicates that the OF has curl topology. Thus, an O-grid is constructed and a contour toolpath is created, as shown in Figure 6(f). The iso-parametric (zigzag) toolpath and the space-filling curve (SFC) toolpath [1] are shown in Figures 6(c)-Figure 6(e). Table 5 shows that the proposed method outperforms the reference methods for all considered measures, i.e., the number of CC points, toolpath length, and machining time. The proposed strategy saves machining time compared to the reference methods. The SFC toolpath is better than the conventional iso-parametric (zigzag) *u* and *v*; however, it is still slower than the proposed method. The virtual machining of the iso-parametric (zigzag-*u*), SFC, and proposed toolpath has been performed in Vericut 7.2 [27]. The machined surfaces are shown in Figure 7. The tool produced by the SFC method includes many turning points so that the SFC closely follows the MRR vectors. However, the tool marks due to the frequent turns jeopardize the quality of the cut. It is worth mentioning that SFC is characterized by variations of the feed rate during sudden changes in the cutting direction.

Similarity at sample points	Template			
	Curl	Star	Spiral	Shear
$\| M_{i,j} - M_0 \|$	**0.1011**	0.1250	0.1261	0.1292
	0.1141	0.1300	0.1280	0.1113
	0.1162	0.1350	0.1382	0.1392
	0.1282	0.1392	0.1468	0.1485

Table 4: Pattern detection for the crown tooth surface.

(a) Crown STL surface toolpath

(b) OF

(c)   Iso-parametric   (*u*)

(d) Iso-parametric (*v*) toolpath

(e) SFC toolpath

(f) Proposed toolpath
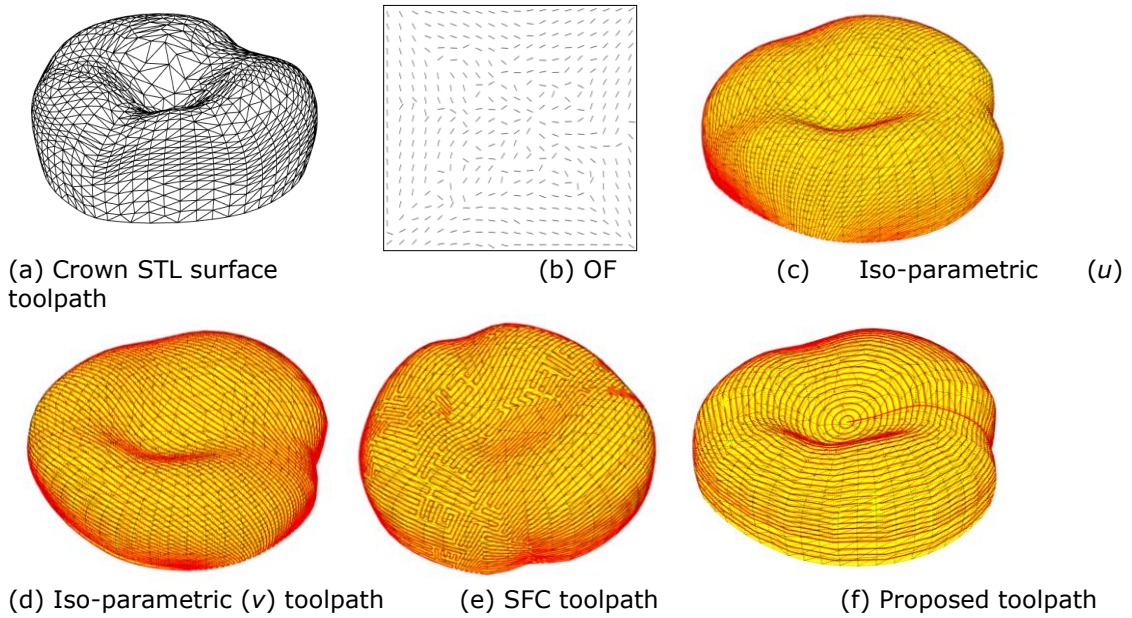
Figure 6: Toolpath for the STL crown of a molar.

Methods	Scallop height, h=0.1 (mm)			
	# of CC points	Length (mm)	Time (s)	Time improvement (%)
Iso-parametric *u*	7388	1.78 10^5	4864	**60.67**
Iso-parametric *v*	6846	1.47 10^5	4744	59.67
SFC	6085	1.59 10^5	3493	45.23
Proposed method	**4446**	**9.40 10^4**	**1913**	-

Table 5: Machining time: Crown for a molar tooth.

(a) Iso-parametric (*u*) toolpath
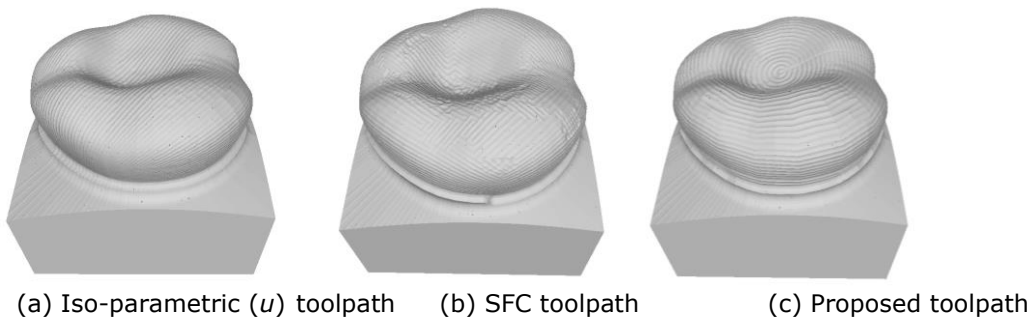
(b) SFC toolpath

(c) Proposed toolpath

Figure 7. Virtual cutting of the dental crown surface.

4 CONCLUSIONS AND RECOMMENDATIONS

This paper offers a novel method of 5-axis machining applied to STL surfaces. The method relies on the detection of efficient machining patterns for the preferred OF. The detection is based on the moment invariants and a library of prescribed templates. A suitable toolpath strategy is selected, based on the classification results. The numerical experiments show that for certain surfaces, the proposed method provides outstanding results compared to several conventional reference methods.

ACKNOWLEDGMENT

Le V. Dang, https://orcid.org/0000-0003-3643-8648
Samart Moodleah, https://orcid.org/0000-0003-0367-5110
Stanislav S. Makhanov, https://orcid.org/0000-0002-1906-0359

REFERENCES

[1]   Anotaipaiboon, W.; Makhanov, S.S.: Tool path generation for five-axis NC machining using adaptive space-filling curves, International Journal of Production Research, 43(8), 2005, 1643–1665. https://doi.org/10.1080/00207540412331322948
[2]   Chen, F.; Zhou, J.; Yang, C.: Reconstructing orientation field from fingerprint minutiae to improve minutiae-matching accuracy, IEEE Transactions on Image Processing, 18(7), 2009, 1665-1670. https://doi.org/10.1109/TIP.2009.2017995
[3]   Chiou, C.J.; Lee, Y.S.: A machining potential field approach to tool path generation for multi-axis sculptured surface machining, Computer-Aided Design, 34(5), 2002, 357–371. https://doi.org/10.1016/S0010-4485(01)00102-6
[4]   Flusser, J.; Zitova, B.; Suk, T.: Moments and Moment Invariants in Pattern Recognition, John Wiley & Sons, Hoboken, NJ, USA, 2009. https://doi.org/10.1002/9780470684757
[5]   Gordon, W.J.; Hall, C.A.: Curvilinear co-ordinate systems and applications to mesh generation, International Journal for Numerical Methods in Engineering, 7(4), 1973, 461–477. https://doi.org/10.1002/nme.1620070405
[6]   Hu, M.K.: Visual pattern recognition by moment invariants, IRE Transactions on Information Theory, 8(2), 1962, 179–187. https://doi.org/10.1109/TIT.1962.1057692
[7]   Hu, P.; Chen, L.; Tang, K.: Efficiency-optimal iso-planar tool path generation for five-axis finishing machining of freeform surfaces, Computer-Aided Design, 83, 2017, 33–50. https://doi.org/10.1016/j.cad.2016.10.001
[8]   Kim, T.; Sarma, S.E.: Toolpath generation along directions of maximum kinematic performance; A first cut at machine-optimal paths, Computer-Aided Design, 34(6), 2002, 453–468. https://doi.org/10.1016/S0010-4485(01)00116-6
[9]   Kumazawa, G.H.; Feng, H.Y.; Barakchi Fard, M.J.: Preferred feed direction field: A new tool path generation method for efficient sculptured surface machining, Computer-Aided Design, 67, 2015, 1–12. https://doi.org/10.1016/j.cad.2015.04.011
[10]   Lasemi, A.; Xue, D.; Gu, P.: Recent development in CNC machining of freeform surfaces: A state-of-the-art review, Computer-Aided Design, 42(7), 2010, 641–654. https://doi.org/10.1016/j.cad.2010.04.002
[11]   Liu, M.; Yap, P.: Invariant representation of orientation fields for fingerprint indexing, Pattern Recognition, 45(7), 2012, 2532–2542. https://doi.org/10.1016/j.patcog.2012.01.014
[12]   Liu, X.; Li, Y.; Li, Q.: A region-based 3 + 2-axis machining toolpath generation method for freeform surface, The International Journal of Advanced Manufacturing Technology, 97(1-4),

2018, 1149-1163. https://doi.org/10.1007/s00170-018-1982-1

[13]   Liu, X.; Li, Y.; Ma, S.; Lee, C.H.: A tool path generation method for freeform surface machining by introducing the tensor property of machining strip width, Computer-Aided Design, 66, 2015, 1–13. https://doi.org/10.1016/j.cad.2015.03.003

[14]   Ma, J.; Song, D.; Jia, Z.; Hu, G.; Su, W.; Si, L.: Tool-path planning with constraint of cutting force fluctuation for curved surface machining, Precision Engineering, 51, 2018, 614–624. https://doi.org/10.1016/j.precisioneng.2017.11.002

[15]   Makhanov, S.S.; Anotaipaiboon, W.: Advanced Numerical Methods to Optimize Cutting Operations of Five-Axis Milling Machines, Springer, Berlin, Heidelberg, Germany, 2007. https://doi.org/10.1007/978-3-540-71121-6

[16]   Moodleah, S.; Bohez, E.J.; Makhanov, S.S.: Five-axis machining of STL surfaces by adaptive curvilinear toolpaths, International Journal of Production Research, 54(24), 2016, 7296–7329. https://doi.org/10.1080/00207543.2016.1176265

[17]   Moodleah, S.; Makhanov, S.S.: 5-Axis machining using a curvilinear tool path aligned with the direction of the maximum removal rate, The International Journal of Advanced Manufacturing Technology, 80(1-4), 2015, 65–90. https://doi.org/10.1007/s00170-015-6958-9

[18]   Rusinkiewicz, S.: Estimating curvatures and their derivatives on triangle meshes, In Proceedings. 2nd International Symposium on 3D Data Processing, Visualization and Transmission, IEEE, 2004, 486–493. https://doi.org/10.1109/TDPVT.2004.1335277

[19]   Schlemmer, M.; Heringer, M.; Morr, F.; Hotz, I.; Bertram, M.H.; Garth, C.; Kollmann, W.; Hamann, B.; Hagen, H.: Moment invariants for the analysis of 2D flow fields, IEEE Transactions on Visualization and Computer Graphics, 13(6), 2007, 1743–1750. https://doi.org/10.1109/TVCG.2007.70579

[20]   Sheffer, A.; Praun, E.; Rose, K.: Mesh parameterization methods and their applications, Foundations and Trends® in Computer Graphics and Vision, 2(2), 2007, 105–171. https://doi.org/10.1561/0600000011

[21]   Shu, C.F.; Jain, R.C.: Vector field analysis, IEEE Transactions on Pattern Analysis and Machine Intelligence, 16(9), 1994, 946–950. https://doi.org/10.1109/34.310692

[22]   Sun, Y.; Xu, J.; Jin, C.; Guo, D.: Smooth tool path generation for 5-axis machining of triangular mesh surface with nonzero genus, Computer-Aided Design, 79, 2016, 60–74. https://doi.org/10.1016/j.cad.2016.06.001

[23]   The Matlab Library: https://www.mathworks.com/products/matlab.html.

[24]   Xu, J.; Sun, Y.; Wang, S.: Tool path generation by offsetting curves on polyhedral surfaces based on mesh flattening, The International Journal of Advanced Manufacturing Technology, 64(9-12), 2013, 1201–1212. https://doi.org/10.1007/s00170-012-4075-6

[25]   Xu, J.; Sun, Y.; Zhang, L.: A mapping-based approach to eliminating self-intersection of offset paths on mesh surfaces for CNC machining, Computer-Aided Design, 62, 2015, 131–142. https://doi.org/10.1016/j.cad.2014.11.010

[26]   Zhang, K.; Tang, K.: An efficient greedy strategy for five-axis tool path generation on dense triangular mesh, The International Journal of Advanced Manufacturing Technology, 74(9-12), 2014, 1539–1550. https://doi.org/10.1007/s00170-014-6083-1

[27]   Vericut Website: https://www.cgtech.com.

[28]   Siemens Website: https://www.plm.automation.siemens.com/global/en/support/docs.html.